Optical and Quantum Electronics (2022) 54:808
https://doi.org/10.1007/s11082-022-04226-1

CPW fed quasi complementary super-wideband MIMO antenna

Deepshikha Lodhi[1] · **Sarthak Singhal**[1]

Received: 26 August 2022 / Accepted: 19 September 2022 / Published online: 30 September 2022

Abstract
A quasi complementary super-wideband antenna element based on coplanar waveguide feeding and having dimensions of 24×22 mm^2 along with an operating range of 3–42.1 GHz (173.3%) is presented in this paper. This structure comprises of a modified F-shaped radiator fed by a tapered feed line and a defected coplanar waveguide ground plane loaded with a slot complementary to the radiator. The pattern and spatial diversity multiple input multiple output configurations of this antenna element have an overall footprint of 24×47 mm^2 and 24×43 mm^2 respectively and both are operating over a frequency range of 2.9–42.14 GHz. At maximum frequencies an intraport isolation ≥ 15 dB and ECC < 0.008 are achieved for both configurations. The lumped RLC equivalent circuit model is also presented for both single element and MIMO configurations. A good agreement between simulated, experimental and equivalent circuit results is obtained.

Keywords Quasi complementary · Super-wideband · Coplanar waveguide fed · MIMO · Spatial diversity · Pattern diversity

1 Introduction

Modern and future wireless communication applications require a compact device with wide bandwidth, high-speed data transmission, and broad system capability. The ultra-wideband (UWB) spectrum allocated by Federal Communication Commission (FCC) (2002) provides high data rate with low power level for short-range communication. To fulfil the demands of wireless communication devices covering both short and long-range communication, researchers initiated efforts to incorporate super-wideband (SWB) technology (Singhal and Singh 2016) into next-generation wireless devices. The literature reports several SWB/UWB antenna structures (Singhal and Singh 2016; Azari 2011; Faouri et al. 2022; Sharma et al. 2018; Ajith and Bhattacharya 2018; Okan 2019; Elhabchi et al. 2020; Kodavanti et al. 2022; Singh et al. 2019; Ur Rahman et al. 2018; Manohar et al. 2014; Maity et al. 2022; Srivastava et al. 2018). The various techniques used to achieve

✉ Sarthak Singhal
sarthak.ece@mnit.ac.in

[1] Department of Electronics and Communication Engineering, Malaviya National Institute of Technology, Jaipur, India

super-wideband performance utilize different radiator geometries (fractal, monopole, dipole, Vivaldi, quasi complementary), diverse feeding techniques (symmetric or asymmetric coplanar waveguide feed, microstrip tapered feed line), different ground structures, parasitic elements etc.

The self-complementary antenna, first discovered by Mushiake (1992), is a well-known broadband antenna that can ideally provide infinite impedance bandwidth because of its complementary structure's constant impedance (188.5 Ω) on an infinitely large ground plane. During the past few years, the self-complementary antenna (SCA) family has gain more importance due to the development of a quasi self-complementary antenna (QSCA) in planar form. A planar QSCA consist a conducting patch, complementary slot, and a built-in impedance matching circuit. To suppress the multipath fading effects occurring in monopole antenna, several multiple-input multiple-output (MIMO) QSCA antennas have been investigated by researchers from both academia and industry. A microstrip fed two port MIMO quasi complementary antenna with inverted T shaped common ground plane for enhanced isolation was presented in Liu et al. 2014a. Another microstrip fed MIMO QSCA was reported in Kaur and Singh (2022) with band rejection characteristics for WiMAX and WLAN bands. In Kumar et al. (2020), a quad element super-wideband QSCA with triple band rejection performance was reported. In Li et al. (2015), a triangular triband quasi complementary antenna for WLAN and WiMAX applications was presented. Several other MIMO antennas with self quasi complementary resonating antenna elements and coplanar waveguide feed are investigated in Raheja et al. (2020), Guo et al. (2010), Lin (2012), Nikam et al. (2022), Dwivedi et al. (2021). Among the previously reported structures (Singhal and Singh 2016; Azari 2011; Faouri et al. 2022; Ur Rahman et al. 2018; Manohar et al. 2014; Maity et al. 2022), due to easy availability and low cost FR-4 epoxy substrate is used by several researchers. In few articles, other substrates like Rogers/RT Duroid (Azari 2011; Singh et al. 2019; Srivastava et al. 2018) having low dielectric losses at millimeter wave frequencies are preferred over FR-4 epoxy substrate. In the previously published geometries either the bandwidth dimension ratio (Balani et al. 2019) is less due to larger dimensions or bandwidth is narrower.

This paper presents a compact quasi-complementary super-wideband antenna and its two MIMO configurations due to the limitations of the abovementioned geometries. Integrating the quasi-complementary radiator, tapered feedline, and defective coplanar waveguide ground plane in the proposed antenna resulted in an impedance bandwidth of ~ 39.1 GHz. In the case of diversity configurations, intra-port isolation of ≥ 20 dB is achieved at maximum operating frequencies without using any decoupling technique. The proposed antenna element, spatial and pattern diversity configurations have achieved a size reduction up to 98%, 67%, and 84%, respectively, over available structures.

2 Antenna design

2.1 Single antenna element

The geometry of the quasi-complementary antenna element (Ant 1) is displayed in Fig. 1a, and the optimized dimensions are listed in Table 1. The proposed antenna is designed and fabricated on a low-cost FR-4 epoxy dielectric substrate of size 24×22 mm^2 and thickness of 1.6 mm. The proposed antenna consists of an F-shaped conducting patch attached to a central strip of tapered CPW feed, a rectangular F-shaped patch

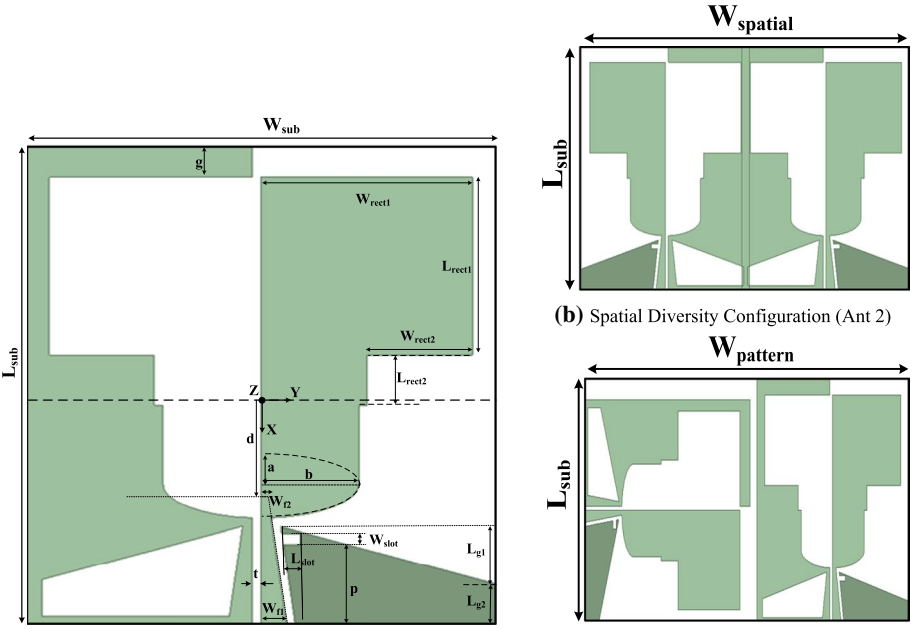

(a) Antenna Element (Ant 1)

(b) Spatial Diversity Configuration (Ant 2)

(c) Pattern Diversity Configuration (Ant 3)

Fig. 1 Geometries of proposed antenna structures

Table 1 Optimised dimensions of proposed antenna configurations

Parameter	L_{sub}	W_{sub}	W_{rect1}	L_{rect1}	W_{rect2}	L_{rect2}	a	b	W_{f1}	W_{f2}
Value	24	22	9.9	9	4.9	2.5	1.7	4.59	1.6	0.375
Parameter	t	L_{g1}	L_{g2}	g	L_{slot}	W_{slot}	d	p	$W_{spatial}$	$W_{pattern}$
Value	0.4	4.88	2	1.5	0.86	0.5	6	4	43	47

loaded with a slightly off-centered radiator's complementary slot and trapezoidal slot, and a supporting trapezoidal ground plane with a rectangular notch. The supporting ground plane acts as the impedance matching circuit that forms part of the in-built CPW feed. The coplanar conducting patch and complementary slots are arranged on the opposite side of the symmetry line.

Since the input impedance of the quasi complementary structure presented by $Z_{in} = \frac{\eta_o}{2} \approx 60\pi \approx 188.5\,\Omega$ Mushiake (2004) has no dependence on frequency or antenna dimensions, therefore quasi self-complementary antenna with extremely large bandwidths can be easily designed by using the self-complementarity principle.

The Riccati equation (Manohar et al. 2014) for a triangularly tapered microstrip-line is solved by $\Gamma(\theta) = \left(\frac{e^{-j\beta L_k}}{2}\right) \ln\left(\frac{Z_L}{Z_o}\right)\left[\frac{\sin(\beta L_k/2)}{(\beta L_k/2)}\right]^2$ where L_k is the length of the tapered microstrip-line, Z_L and Z_0 are the respective load impedance and characteristic impedance, and $\Gamma(\theta)$ is the reflection coefficient and β is the phase constant. As a result, the triangular tapered microstrip line's impedance changes over its length. The standard 50

Ω (coaxial) RF source and the quasi-complementary radiator are impedance matched using a tapered feed-line.

Figure 2 shows the various design steps of an antenna element. A monopole antenna with a coplanar waveguide feed is designed initially in Step 1. The radiator is designed by combining three rectangular sections of different dimensions and one elliptical section. The quasi-complementary radiator of Step 2 is designed by dividing the radiator of Step 1 into 2 subsections and replacing the left half subsection with the complement of right half section resulting into self-complementary configuration. This resulted into wider impedance bandwidth. Since the dimensions of main F shaped radiating patch are slightly different from its complementary slot, hence the antenna is termed as quasi complementary. Furthermore, in step 3, the rectangular feedline and rectangular ground plane are replaced with one side tapered feedline and trapezoidal ground plane without affecting the gap between the two. This replacement of feedline and ground plane sections was carried out to provide smooth current flow leading to minimized incident wave's reflections resulting into improved impedance matching between the quasi-complementary radiator and the standard 50 Ω (coaxial) RF source and enhanced impedance bandwidth. The tapered feed line allows steady impedance variations over the frequency range, and the impedance can be estimated using Manohar et al. (2014). At higher frequencies, to reduce the electromagnetic coupling between the ground plane and the radiator, a trapezoidal slot is created in step 4, complementary to the shape of the right side trapezoidal ground plane. In final stage i.e. Ant 1, theright hand side trapezoidal ground plane is loaded with a rectangular notch to improve the impedance matching in the frequency range of 29.8–31.8 GHz and 42.4–44.8 GHz by exciting additional resonances at 30.8 GHz and 33.2 GHz.

2.2 MIMO

The spatial diversity MIMO antenna (Ant 2), shown in Fig. 1b, is created by aligning two identical antenna elements in a mirror image configuration and overlapping some ground plane region of ground plane. It has an overall dimension of 24×43 mm^2. In the pattern diversity configuration (Ant 3), Fig. 1c, the two antenna elements are orthogonal to each other, with a horizontal separation of 1 mm between them. It has an overall footprint of 24×47 mm^2. The fabricated prototypes of Ant 1, Ant 2 and Ant 3 are illustrated in Fig. 3. The proposed antenna is simulated and analysed with the Finite Element Method-based ANSYS v 21 software (HFSS 2021).

(a) Step 1 **(b)** Step 2 **(c)** Step 3 **(d)** Step 4 **(e)** Ant 1

Fig. 2 Design Steps of the proposed antenna element

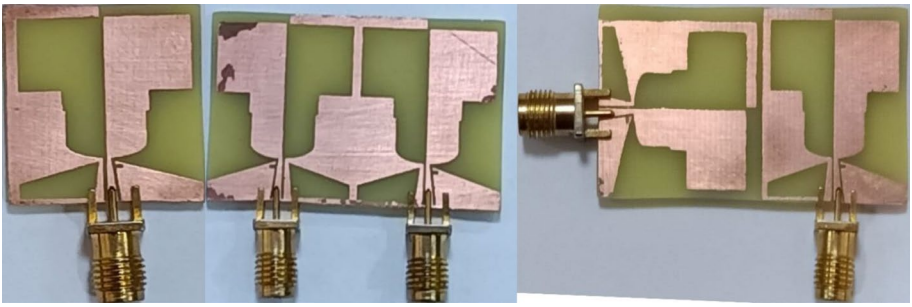

(a) Single element **(b)** Spatial Diversity **(c)** Pattern Diversity

Fig. 3 Proposed antenna prototypes

3 Result and discussion

3.1 Frequency domain results

3.1.1 Single antenna element

The validation of simulated scattering parameters with experimental results is done upto 40 GHz and the radiation pattern and gain measurement is done upto 18 GHz due to measurement setup limitations. The intermediate antenna element design stages are compared in terms of their VSWR characteristics in Fig. 4 and the quantitative analysis of bands of each intermediate stage is listed in Table 2. It is observed that Step 1 antenna has two operating bands with frequency range of 29.7–34 GHz and 39.4 GHz to more than 44 GHz. In case of Step 2 antenna, the lower band edge frequency of first operating band reduces from 29.7 to 3.2 GHz due to the inherent wideband property of quasi complementary structure. This antenna structure is operating over four bands i.e.3.2–28.8 GHz, 31–31.8 GHz, 32.6–36.6 GHz and 38.2–42.4 GHz. For Step 3 antenna, the tapering of the outer edge of feedline and inner edge of right-side ground plane improved the impedance matching

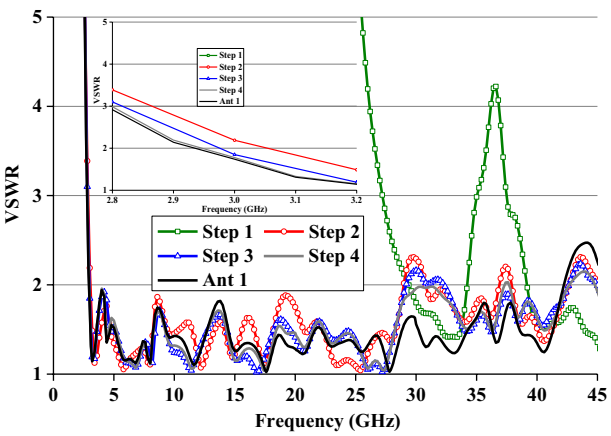

Fig. 4 VSWR of design stages of antenna element

Table 2 Comparison of intermediate stages of the Ant.1

Band	Step 1	Step 2	Step 3	Step 4	Ant 1
Band 1					
f_{l1} (GHz)	29.39	3.05	2.98	2.95	2.94
f_{h1} (GHz)	34.23	28.98	29.18	37.32	42.22
Band 2					
f_{l2} (GHz)	39.17	30.78	32.3	37.68	–
f_{h2} (GHz)	> 44	36.89	42.63	42.67	–
Band 3					
f_{l3} (GHz)	–	37.91	–	–	–
f_{h3} (GHz)	–	42.65	–	–	–

resulting into two operating bands 2.98–29.18 GHz and 32.3–42.63 GHz instead of four operating bands. In case of Step 4 antenna, the loading of the left hand side ground plane with a trapezoidal slot improved the impedance matching near the frequencies of 30 GHz and 37.5 GHz leading to enhancement of bandwidth for first operating band from 26.2 to 34.37 GHz and reduction in the bandwidth of second operating band from 10.33 to 4.99 GHz. In the last stage antenna i.e. Ant 1, the introduction of a rectangular notch on the right hand side ground plane merged both the operating bands of Step 4 into a single super wideband2.94–42.22 GHz. The comparison of simulated VSWR of Ant1 with experimental results is depicted in Fig. 5. The slight deviations in simulated and experimental results at higher frequenciescan be attributed to the fabrication tolerancesand measurement errors.

The input impedance vs frequency plot is shown in Fig. 6. The real part of input impedance is varying around 50 Ω and imaginary part is oscillating around 0 Ω. This results in an overall impedance matching of 50 Ω in the entire opearting band. From Fig. 7, it is observed that the normalized radiation patterns are bidirectional in E (or XZ)-plane and omni directional in H (or YZ)-plane at frequencies below 10 GHz however at higher frequencies > 10 GHz, distorted radiation patterns are observed due to the exciation of higher order modes. The peak realized gain is observed to be varying in the range of 2–8.6 dBi. Maximum radiation efficiency of 97.3% is achieved in the entire operating band as depicted in Fig. 8. Table 3 lists the comparison of Ant 1 with

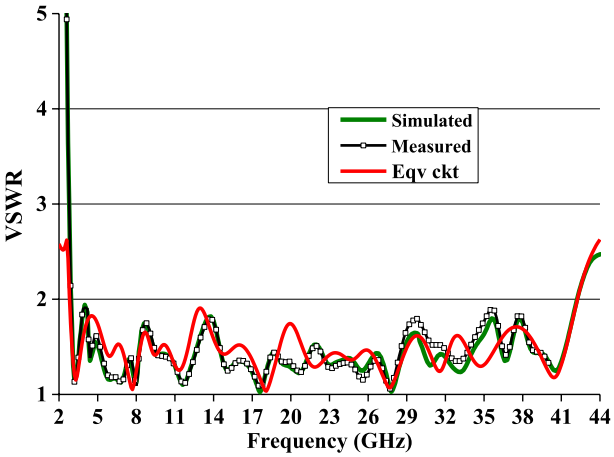

Fig. 5 VSWR plot of Ant 1

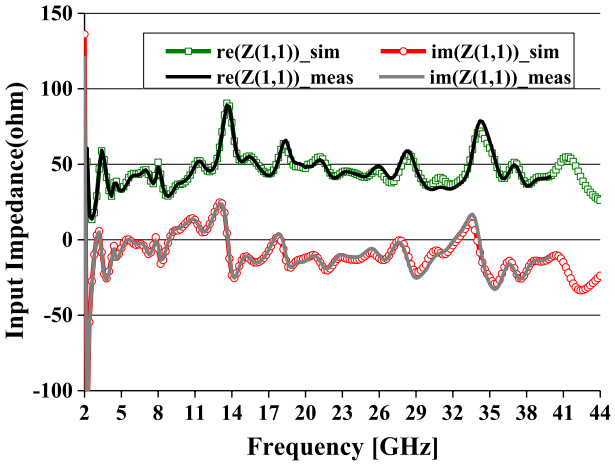

Fig. 6 Input Impedance plot of Ant 1

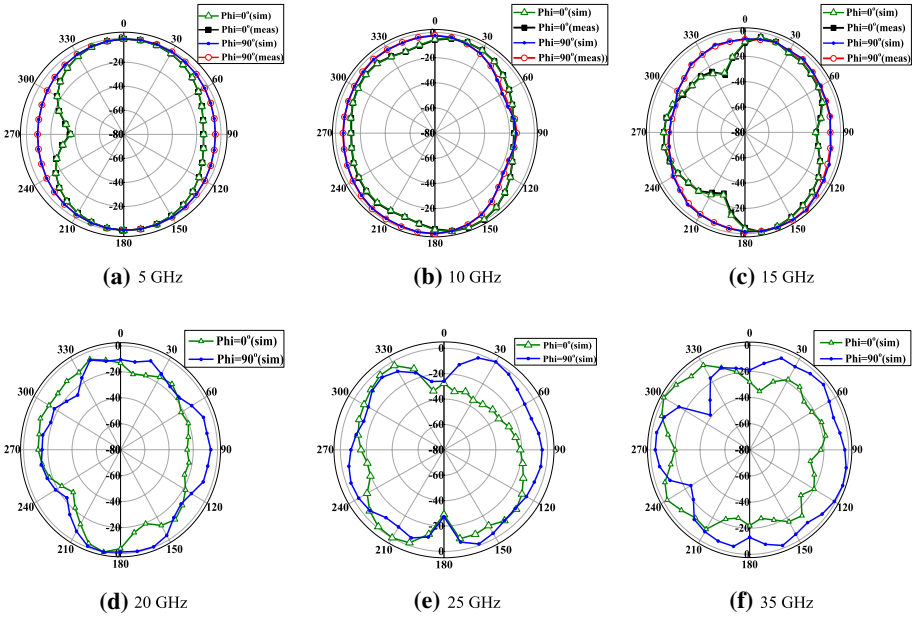

(a) 5 GHz **(b)** 10 GHz **(c)** 15 GHz

(d) 20 GHz **(e)** 25 GHz **(f)** 35 GHz

Fig. 7 Radiation pattern of proposed single antenna element (Ant 1)

previously reported structures in terms of their dimensions, percentage size reduction in terms of square of wavelength at lowest band edge frequency, peak realized gain and bandwidth dimension ratio. The proposed antenna is observed to be having a size reduction upto ~ 98% with dimensions of 0.24 $\lambda_L \times 0.22\ \lambda_L$, comaparble peak gain of 8.6 dBi, maximum BDR of ~ 3284 and comparable fracational bandwidth of ~ 174% in comaprison to other comapred geometries.

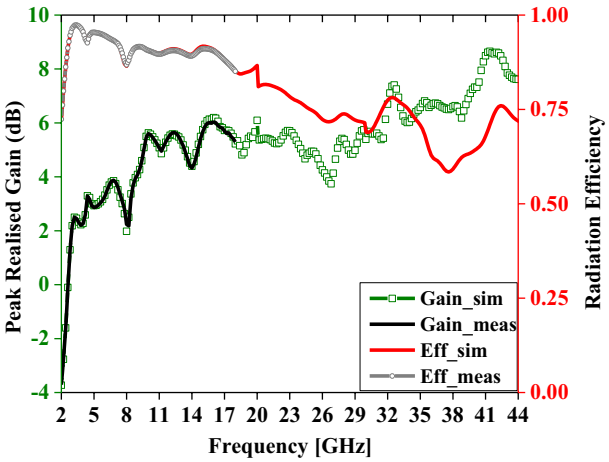

Fig. 8 Gain and radiation efficiency of proposed single antenna element (Ant1)

3.1.2 MIMO

3.1.2.1 Spatial diversity configuration The reflection coefficient plots for both ports of spatial diversity configuration, i.e. S11 ≅ S22, are overlapping in Fig. 9a due to identical antenna elements. The intraport isolation between the antenna elements is more than the required value of 13 dB (Ahmed et al. 2018) in the entire operating frequency range except for frequency range of 4.3–4.7 GHz where due to electromagnetic coupling the isolation is reducing upto ~ 10 dB and is more than 20 dB at frequencies higher than 20 GHz. The impedance bandwidth of proposed MIMO spatial diversity configuration is 2.91–42.14 GHz. No additional isolation structure is added as the geometry of proposed quasi complementary antenna is itself acting as an isolation structure. The ground planes are connected to achieve the same reference voltage. Due to identical antenna elements, the radiation patterns for port 1 and port 2 are also same. Therefore, the radiation patterns in E- and H- planes are shown for Port 1 only in Fig. 10. The radiation patterns are bidirectional in E-plane and omnidirectional in H-plane at frequencies lesser than 10 GHz. At frequencies more than 10 GHz, the radiation patterns in both planes get distorted due to the excitation of higher order modes.

3.1.2.2 Pattern diversity configuration Both elements of the pattern diversity configuration have an impedance bandwidth of 2.9–42.1 GHz and the intra-port isolation, S21 > 13 dB in the entire operating band and S21 > 25 dB in the majority of the operating band, as shown in Fig. 11. The radiation pattern achieved for port 1 in XZ plane is same as pattern of port 2 in YZ plane and vice versa as shown in Figs. 12 and 13. This interchanging of planes confirms pattern diversity is achieved.

3.1.2.3 Equivalent circuit modelling The equivalent circuit model of single element (Ant 1), spatial diversity antenna (Ant 2) and pattern diversity antenna (Ant 3) is shown Fig. 14 and the optimised value of R, L and C are tabulated in Table 4. The equivalent circuit for narrow band antenna is approximately modelled by LC resonant circuit. Unlike narrow band antenna, a good approximation to represent ultrawideband or super-wideband antenna is the cascaded connection of multiple parallel RLC resonant circuits. This cascading of RLC resonant circuit results in wide band in UWB/SWB antenna due to the continuously overlapping of adjacent

Table 3 Comparison of Ant1 element with previously reported structures

S. No	Ant	Bandwidth			Dimensions in terms of		% size reduction in terms of λ_L^2	Peak Gain (dBi)	BDR
		In GHz	Ratio:1	% BW	(mm^2)	(λ_L^2)			
1	Elhabchi et al. (2020)	3–20	6.67	147.83	30×30	0.3 λ_L×0.3 λ_L	21.78	6	1642.56
2	Kodavanti et al. (2022)	5.54–80	14.4	174.4	18×12	0.32 λ_L×0.21 λ_L	25.93	8	2447.71
3	Ur Rahman et al. (2018)	1.7–30	17.65	178.55	54.25×57.7	0.31 λ_L×0.33 λ_L	31.18	5.8	1745.36
4	Ajith and Bhattacharya (2018)	0.420–5.5	13.1	171.62	230×230	0.32 λ_L×0.32 λ_L	31.25	5.2	1675.98
5	Singh et al. (2019)	3.36–39.61	11.79	168.72	27×32	0.3 λ_L×0.36 λ_L	34.81	6.2	1562.22
6	Okan (2019)	3.4–37.4	11	166.67	30×28	0.32 λ_L×0.34 λ_L	35.29	11	1531.89
7	Elhabchi et al. (2020)	2.59–31.14	12.02	169.29	40×40	0.35 λ_L×0.35 λ_L	42.53	4.8	1381.96
8	Azari (2011)	3–21.5	7.17	151.02	38×36	0.38 λ_L×0.36 λ_L	48.54	5	1103.95
9	Faouri et al. (2022)	3.37–27.51	8.16	156.3	36×36	0.40 λ_L×0.40 λ_L	67.7	7.6	956.02
10	Sharma et al. (2018)	3.4–9.6	2.82	95.38	45×38.9	0.51 λ_L×0.44 λ_L	68.63	7.56	425.04
11	Azari (2011)	10–50	5	133.33	60×60	2 λ_L×2 λ_L	98.24	9.2	33.33
12	Ant 1	3–42.1	14.03	173.3	24×22	0.24 λ_L×0.22 λ_L	–	8.6	3283.95

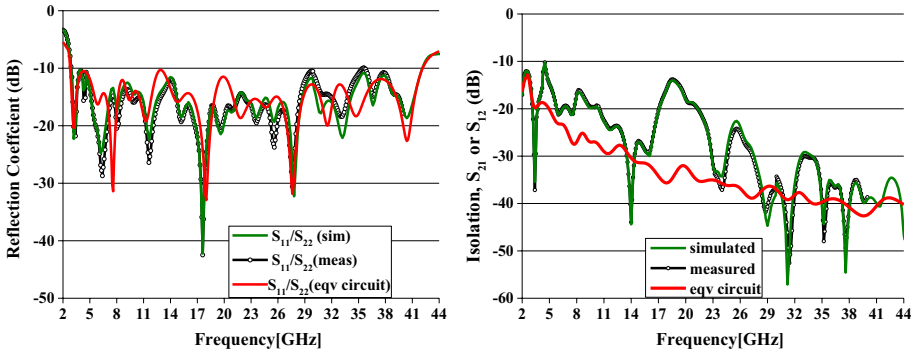

(a) Reflection Coefficient **(b)** Isolation

Fig. 9 Scattering parameters of Spatial diversity configuration

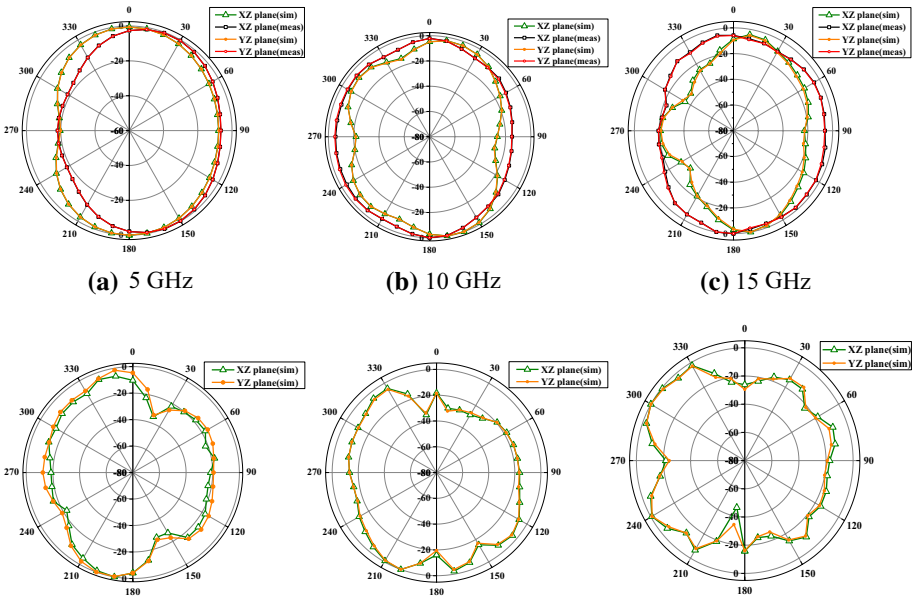

(a) 5 GHz **(b)** 10 GHz **(c)** 15 GHz

(d) 20 GHz **(e)** 25 GHz **(f)** 35 GHz

Fig. 10 Radiation patterns of spatial diversity MIMO configuration

resonances (Chu and Yang Dec. 2008). The lumped equivalent circuit model of proposed Ant1 is represented by a series connection of eighteen series resonant circuit (N = 18) with inductor (L_f), resistor (R_f) and capacitor (C_f). The series connection of L_f, C_f and R_f represents the effect of feeding and higher order modes.

$$Q = \frac{f_r}{Bandwidth} = 2\pi f_r CR \tag{1}$$

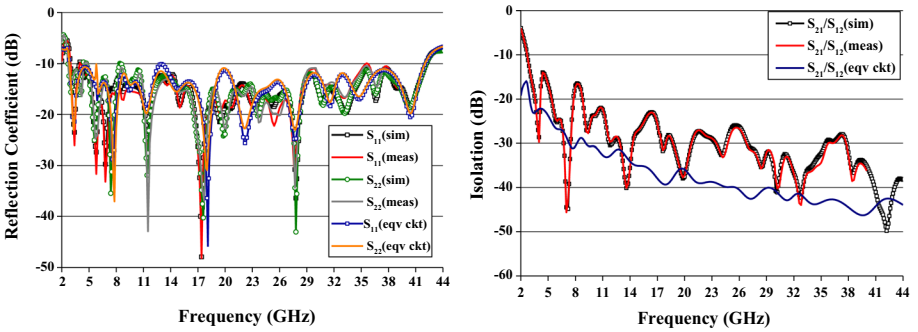

(a) Reflection Coefficient **(b)** Intra port Isolation

Fig. 11 Scattering parameters of pattern diversity configuration

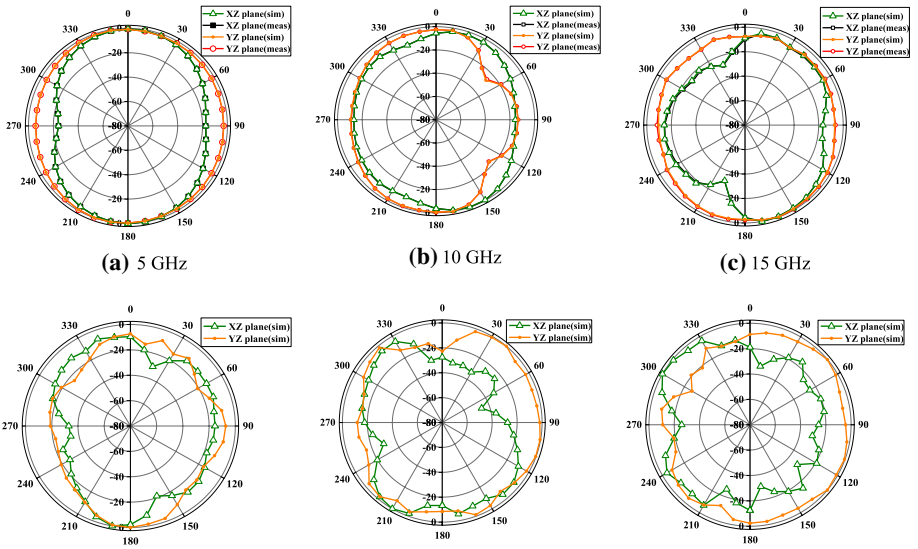

(a) 5 GHz **(b)** 10 GHz **(c)** 15 GHz

(d) 20 GHz **(e)** 25 GHz **(f)** 35 GHz

Fig. 12 Radiation patterns of port1 of pattern diversity MIMO configuration

$$f_r = \frac{1}{2\pi\sqrt{LC}} \tag{2}$$

The circuit is excited by 50 Ω RF source. ANSYS circuit simulator v21 is used to simulate and analyse this circuit. To model the lumped equivalent circuit of proposed antenna the value of real and imaginary part of input to impedance, Z_{11} corresponding to resonant frequency of proposed antenna is extracted from the plot generated by HFSS EM simulator. The Eqs. (1–2) are used to calculate the value of L and C corresponding to each resonant frequency (Maity et al. 2022). The calculated value of L and C are further tuned and

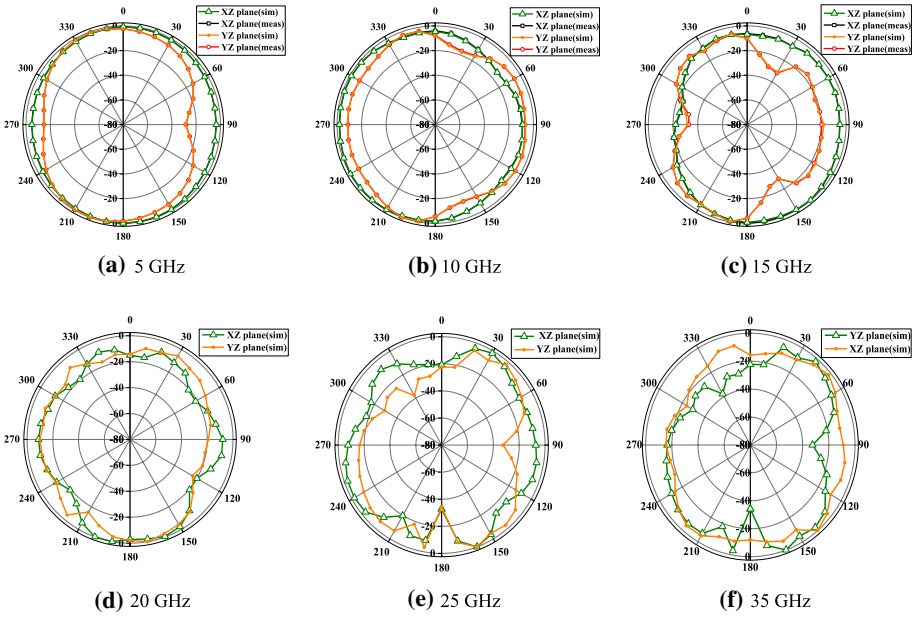

Fig. 13 Radiation patterns of port2 of pattern diversity MIMO configuration

optimised using ANSYS circuit simulator to get the desired response. In case of spatial diversity antenna (Ant 2), the equivalent circuit for each antenna element will remain same as Ant1 as both the elements are identical. However, to consider the effect of coupling between the two elements with connected ground plane a inductor ($L_{spatial}$) is connected in parallel with capacitor ($C_{spatial}$) (Abdulhasan et al. 2021). For Ant 3, the coupling between the two orthogonal placed antenna elements is modelled by parallel connection of inductor ($L_{pattern}$) capacitor ($C_{pattern}$) (Iqbal et al. 2020). The equivalent circuit model for Ant 3. The results of equivalent circuit model for Ant 1, Ant 2 and Ant 3 are depicted in Fig. 14. These results agree well with simulated and measured results, and in accordance with previously reported results in Faouri et al. (2022), Maity et al. (2022), Mohanty (2021).

3.1.2.4 MIMO diversity performance The diversity performance of MIMO antenna configurations is evaluated in terms of the following parameters using standard equations from Ahmed et al. (2018), Lodhi and Singhal (2021). Envelope correlation coefficient (ECC) is used to estimate the amount of correlation between the two elements of MIMO antenna. It can be calculated by using (3) based on scattering parameters or by using (4) based on far-field radiation patterns. Figure 15a illustrates that for both spatial (ECC < 0.009) and pattern (ECC < 0.017) diversity configurations, ECC is ≤ 0.002 at maximum operating frequencies and ≤ 0.05 in entire band of operation. The maximum acceptable value of ECC is 0.5. The maximum value of ECC calculated using farfield (Fig. 15b) is 0.05 for spatial and 0.01 for pattern diversity configuration. The diversity gain (DG), ≅ 10 (acceptable) at all operating frequencies for both configurations as illustrated in Fig. 15(c). In addition to this, the channel capacity loss shown in Fig. 15d is also < 0.4 b/sec/Hz. From Fig. 16a, b, it is observed that the mean effective gain is − 3 dB as desired for both the MIMO configurations. The MEG difference between the two ports of MIMO antenna is also nearly 0 dB. These ECC and CCL values are less than the acceptable limits, and the almost constant values of DG

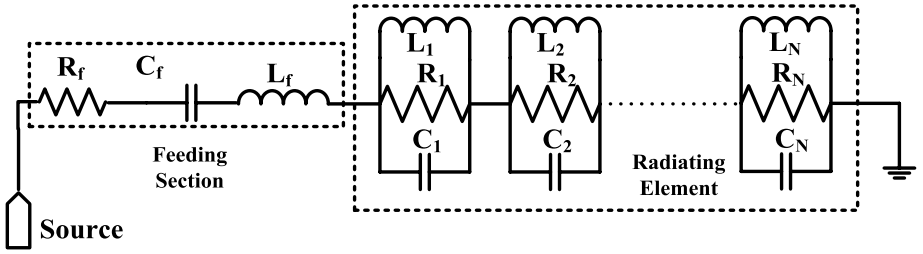

(a) Single antenna element(Ant1)

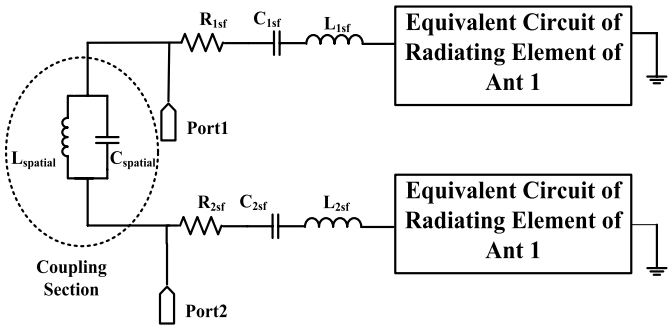

(b) Spatial diversity Antenna(Ant2)

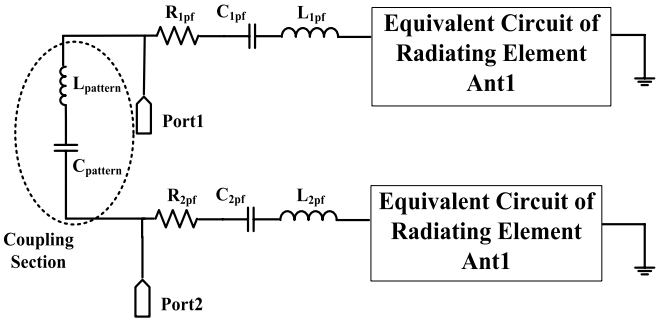

(c) Pattern diversity Antenna(Ant 3)

Fig. 14 Equivalent circuit model for all three proposed configurations

and MEG indicate that the proposed antenna configurations are suitable for SWB MIMO applications.

$$ECC(\rho_{ij})\Big|_{Based\ on\ scattering\ parameters} = \frac{\left|S_{ii}^{*}S_{ij} + S_{ji}^{*}S_{jj}\right|^{2}}{\left(1 - \left|S_{ii}\right|^{2} - \left|S_{ji}\right|^{2}\right)\left(1 - \left|S_{jj}\right|^{2} - \left|S_{ij}\right|^{2}\right)} \quad (3)$$

Table 4 Optimized value of *R*, *L*, *C* components for equivalent circuit models

L	L_1	L_2	L_3	L_4	L_5	L_6	L_7
Value (pH)	1297.36	320.36	185.72	324.74	98.27	79.58	259.38
L	L_8	L_9	L_{10}	L_{11}	L_{12}	L_{13}	L_{14}
Value (pH)	937.40	46.13	40.29	44.19	68.56	25.88	11.68
L	L_{15}	L_{16}	L_{17}	L_{18}	$L_f=L_{1sf}=L_{2sf}=L_{1pf}=L_{2pf}$	$L_{spatiaL}$	$L_{patteRn}$
Value (pH)	13.84	14.48	9.26	20.68	97.5	12,835	19,627
C	C_1	C_2	C_3	C_4	C_5	C_6	C_7
Value (pF)	2.94	11.20	3.20	4.32	3.43	3.14	0.61
C	C_8	C_9	C_{10}	C_{11}	C_{12}	C_{13}	C_{14}
Value (pF)	1.257	2.25	1.62	1.09	2.28	1.15	1.24
C	C_{15}	C_{16}	C_{17}	C_{18}	$C_f=C_{1sf}=C_{2sf}=C_{1pf}=C_{2pf}$	$C_{spatiaL}$	$C_{patteRn}$
Value (pF)	2.82	0.932	2.61	0.94	2.40	1×10^{-15}	5.67
R	R_1	R_2	R_3	R_4	R_5	R_6	R_7
Value (Ω)	58.84	51	32.58	20.47	40.60	29.46	28.36
R	R_8	R_9	R_{10}	R_{11}	R_{12}	R_{13}	R_{14}
Value (Ω)	55.87	25.06	38.13	31.06	12.37	22.51	43.82
R	R_{15}	R_{16}	R_{17}	R_{18}	$R_f=R_{1sf}=R_{2sf}=R_{1pf}=R_{2pf}$		
Value (Ω)	47.05	12.37	31.06	38.13	5.7		

$$ECC(\rho_{ij})\Big|_{Based\ on\ farfield} = \frac{\iint_{4\pi} E_i(\theta,\Phi)\cdot E_j^*(\theta,\Phi)d\Omega}{\sqrt{\iint_{4\pi} E_i(\theta,\Phi)\cdot E_i^*(\theta,\Phi)d\Omega \iint_{4\pi} E_j(\theta,\Phi)\cdot E_j^*(\theta,\Phi)d\Omega}} \quad (4)$$

The comparison of Ant2 and Ant3 with previously reported other 2 element MIMO antenna configurations are provided in Table 5. It displays that both the proposed MIMO configurations have sufficient isolation of ≥ 15 dB at maximum operating frequencies with very low values of ECC and superwide bandwidth of ~ 39 GHz (~ 174%). In addition to this, Ant 2 has achieved a size reduction of 67% and Ant 3 has achieved a size reduction of ~ 84% over previously reported structures.

4 Conclusion

A quasi-complementary radiator, tapered feed line, and coplanar waveguide ground plane are used in this paper to achieve super wide band performance. The super wide bandwidth achieved by the quasi-complementary antenna and its MIMO configuration is 3–42.1 GHz and 2.9–42.14 GHz, respectively. It has a high BDR of 3283.9, a peak gain of 8.6 dBi, and a maximum radiation efficiency of 97.3 percent. The intraport isolation for both the MIMO configurations is ≥ 15 dB in major portion of the operating band. The equivalent circuit model for Ant1, Ant2 and Ant3 is also presented to discuss the mechanism of UWB and SWB antenna. The above-mentioned advantages of proposed antenna configurations make it suitable for various super-wideband applications.

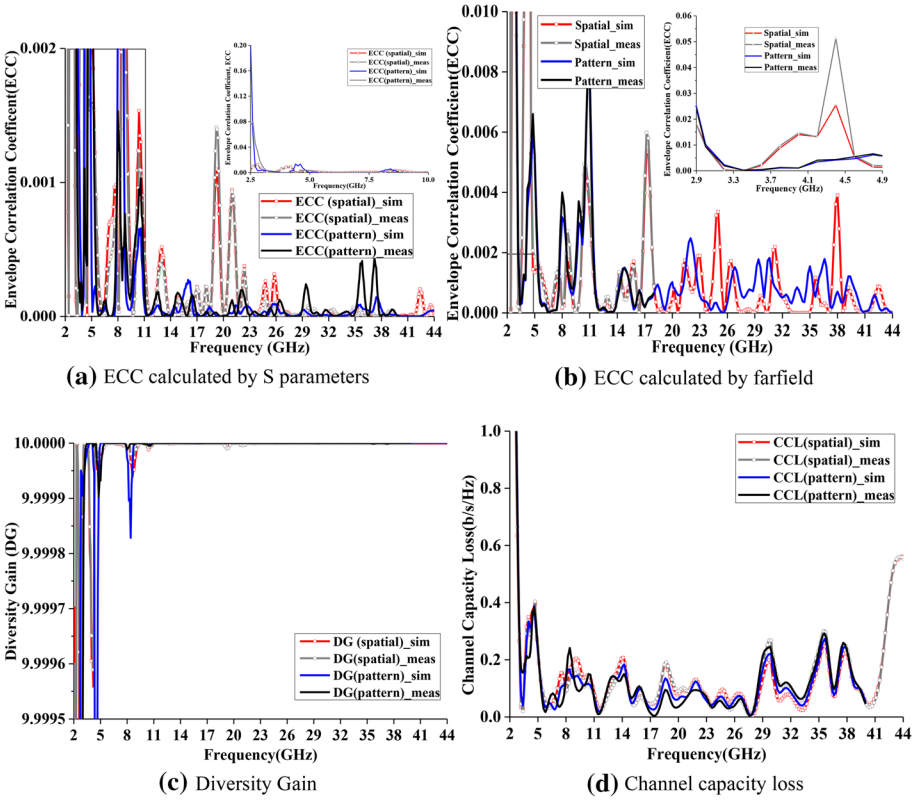

(a) ECC calculated by S parameters **(b)** ECC calculated by farfield

(c) Diversity Gain **(d)** Channel capacity loss

Fig. 15 Diversity performance parameters for MIMO configuration

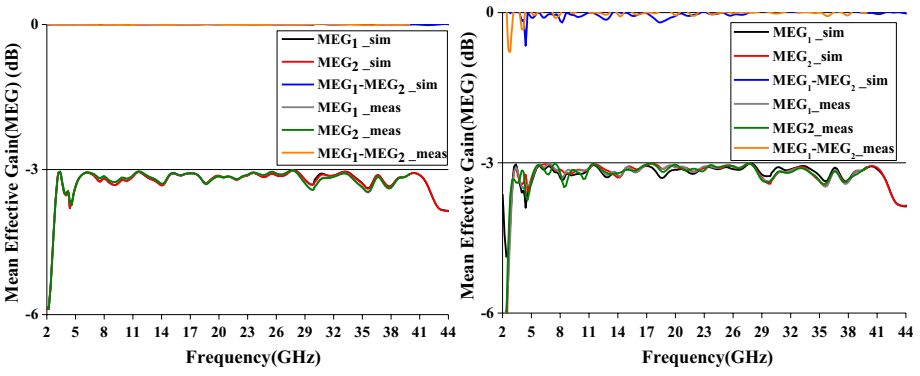

(a) Spatial **(b)** Pattern

Fig. 16 Mean effective gain for MIMO configuration

Table 5 Comparison of proposed spatial and MIMO diversity configuration with other reported structures

References	Bandwidth		Dimension in terms of		% Size reduction (λ_L^2)	Maximum ECC	Isolation (dB) in major portion of operating band	No. of ports	Ground
	GHz	%	(mm^2)	λ_L^2					
Hong et al. (2008)	2.27–10.2	127.19	81×42	0.61 λ_L×0.45 λ_L	45	–	15	2	CG
Oni et al. (2015)	2.2473–30	172.12	81×42	0.34 λ_L×0.67 λ_L	67	–	11	2	CG
Liu et al. (2014b)	3.1–10.6	109.49	40×60	0.41 λ_L×0.62 λ_L	62	0.03	15	2	CG
Chang et al. (2019)	7.87–12.08	42.21	39×17.5	1.02 λ_L×0.46 λ_L	46	0.001	20	2	NCG
Ahmed et al. (2018)	3.1–20	146.32	84×52	0.87 λ_L×0.54 λ_L	54	–	20	2	NC
Mao et al. (2013)	3.1–10.6	109.49	60×40	0.62 λ_L×0.41 λ_L	41	0.06	20	2	CG
Kong et al. (2016)	2.85–11.8	122.18	50×50	0.48 λ_L×0.48 λ_L	48	0.012	14	2	CG
Toktas (2017)	2.2–13.3	143.23	50×82	0.37 λ_L×0.6 λ_L	60	0.04	15	2	CG
Radhi et al. (2018)	3.1–10.6	109.49	93×47	0.96 λ_L×0.49 λ_L	49	–	20	2	CG
Lodhi and Singhal (2021)	3.45–52.2	175.2	28×53	0.32 λ_L×0.61 λ_L	61	0.03	15	2	NCG
Patre and Singh (2016)	2.2–13.1	142.4	66.8×40	0.48 λ_L×0.29 λ_L	34.3	–	–	2	CG
Ant 2	**2.91–42.14**	**174.2**	**24×43**	**0.23 λ_L×0.41 λ_L**	**-**	**0.009**	**15**	**2**	**CG**
Chacko et al. (2013)	2.8–11	118.84	58×58	0.54 λ_L×0.54 λ_L	64.5	–	14	2	CG
Gallo et al. (2012)	3–12	120	80×80	0.8 λ_L×0.8 λ_L	83.8	–	15	2	CG
Mohanty and Ranjan Behera (2021)	2.4–10.2	115.33	32×64	0.68 λ_L×0.77 λ_L	80.2	0.15	20	2	CG
Srivastava et al. (2018)	3.2–11.2	111.11	81×42	0.86 λ_L×0.45 λ_L	73.2	0.015	13	2	NCG
Ahmed et al. (2018)	3.1–20	146.32	93×56	0.96 λ_L×0.58 λ_L	81.4	–	20	2	NCG
Lodhi and Singhal (2021)	3.1–52.2	177.58	48×45	0.47 λ_L×0.5 λ_L	55.9	15	0.03	2	NCG
Ant 3	**2.97–42.14**	**174.2**	**24×47**	**0.23 λ_L×0.45 λ_L**	–	**0.017**	**15**	**2**	**NCG**

CG Connected ground, *NCG* Not Connected Ground

The proposed antenna geometry names are indicated in bold

Acknowledgements Not applicable.

Author contributions All authors contributed to the study conception, design, material preparation, data collection, analysis and writing of the manuscript.

Funding The authors declare that no funds, grants, or other support were received during the preparation of this manuscript.

Availability of data and materials Data sharing not applicable to this article as no datasets were generated or analysed during the current study.

Declarations

Competing interests The authors declare no competing interests.

Conflict of interest The author has no relevant financial or non-financial interests to disclose.

Ethical approval Not Applicable.

Consent to participate Not applicable.

Consent for publication Not applicable.

Human participants and/or animals Not applicable.

Informed consent All authors are informed.

References

Abdulhasan, R.A., Alias, R., Ramli, K.N., Seman, F.C., Abd-Alhameed, R.A., Jawhar, Y.A.: Directional and isolated uwb-mimo antenna-based Uniplanar uwb-fss array and t-strip for Bi-Static Microwave Imaging: baggage-scanner. Int. J. RF Microw. Comput. Aided Eng. (2021). https://doi.org/10.1002/mmce.22960

Ahmed, B.T., Olivares, P.S., Campos, J.L., Vázquez, F.M.: (3.1–20) ghzmimo antennas. AEU-Int. J. Electron. Commun. **94**, 348–358 (2018)

Ajith, K.K., Bhattacharya, A.: A novel compact super-wideband bowtie antenna for 420 MHz to 5.5 ghz operation. IEEE Trans. Antennas Propag. **66**(8), 3830–3836 (2018)

Azari, A.: A new super wideband fractal microstrip antenna. IEEE Trans. Antennas Propag. **59**(5), 1724–1727 (2011)

Balani, W., Sarvagya, M., Ali, T., Pai, M., Anguera, J., Andujar, A., Das, S.: Design techniques of super-wideband antenna–existing and future prospective. IEEE Access **7**, 141241–141257 (2019)

Chacko, B.P., Augustin, G., Denidni, T.A.: Uniplanar slot antenna for Ultrawideband polarization-diversity applications. IEEE Antennas Wirel. Propag. Lett. **12**, 88–91 (2013)

Chang, Y., Liu, Q., Tang, X., Du, G., Li, G., Cheng, D.: Compact MIMO antenna with high isolation characteristic for UWB portable applications. Microw. Opt. Technol. Lett. **62**(3), 1391–1397 (2019)

Chu, Q., Yang, Y.: A compact ultrawideband antenna with 3.4/5.5 GHz dual band-notched characteristics. IEEE Trans. Antennas Propag. **56**(12), 3637–3644 (2008). https://doi.org/10.1109/TAP.2008.2007368

Dwivedi, A.K., Sharma, A., Singh, A.K., Singh, V.: Metamaterial inspired dielectric resonator MIMO antenna for isolation enhancement and linear to circular polarization of waves. Measurement **182**, 109681 (2021)

Elhabchi, M., Srifi, M.N., Touahni, R.: A novel modified U-shaped microstrip antenna for Super Wide Band (SWB) applications. Analog Integr. Circ. Sig. Process **102**(3), 571–578 (2020)

Faouri, Y., Ahmad, S., Naseer, S., Alhammami, K., Awad, N., Ghaffar, A., Hussien, M.: Compact super wideband frequency diversity hexagonal shaped monopole antenna with switchable rejection band. IEEE Access (2022). https://doi.org/10.1109/ACCESS.2022.3167387

Federal Communications Commission (FCC). Revision of part 15 of the commission's rules regarding ultra-wideband transmission systems first rep. and order, ET Docket 98–153, FCC 02-48, Adopted: Feb. 2002; Released. (2002)

Gallo, M., Antonino-Daviu, E., Ferrando-Bataller, M., Bozzetti, M., Molina-Garcia-Pardo, J.M., Juan-Llacer, L.: A broadband pattern diversity annular slot antenna. IEEE Trans. Antennas Propag. **60**(3), 1596–1600 (2012)

Guo, L., Wang, S., Chen, X., Parini, C.G.: Study of compact antenna for UWB applications. Electron. Lett. **46**(2), 115 (2010)

HFSS: High frequency structure simulator. ANSYS Electronics Suite 2021R1, Ansys Corporation, available: http://www.ansys.com

Hong, S., Chung, K., Lee, J., Jung, S., Lee, S.-S., Choi, J.: Design of a diversity antenna with stubs for UWB applications. Microw. Opt. Technol. Lett. **50**(5), 1352–1356 (2008)

Iqbal, A., Smida, A., Alazemi, A.J., Waly, M.I., Khaddaj Mallat, N., Kim, S.: Wideband circularly polarized MIMO antenna for high data wearable biotelemetric devices. IEEE Access **8**, 17935–17944 (2020). https://doi.org/10.1109/ACCESS.2020.2967397

Kaur, H., Singh, H.S., Upadhyay, R.: Design of a compact quasi-self-complementary UWB-MIMO antenna with dual band-notched characteristics for wireless communication applications. Int. J. Electron. (2022). https://doi.org/10.1080/00207217.2022.2065536

Kodavanti, P.V., Jayasree, P.V., Bhima, P.R.: Design and analysis of Super Wide Band antenna and its notch band characteristics. Soft. Comput. **26**(9), 4275–4287 (2022)

Kong, Y., Li, Y., Yu, K.: A minimized MIMO-UWB antenna with high isolation and triple band-notched functions. Frequenz (2016). https://doi.org/10.1515/freq-2016-0108

Kumar, P., Urooj, S., Malibari, A.: Design and implementation of quad-element super-Wideband MIMO antenna for IOT applications. IEEE Access **8**, 226697–226704 (2020)

Li, H., Kang, L., Wang, X.H., Yin, Y.-Z.: Design of tri-band quasi-self-complementary antenna for WLAN and WIMAX applications. Progr. Electromagn. Res. Lett. **56**, 89–94 (2015)

Lin, C.-C.: Compact bow-tie quasi-self-complementary antenna for UWB applications. IEEE Antennas Wirel. Propag. Lett. **11**, 987–989 (2012). https://doi.org/10.1109/LAWP.2012.2214021

Liu, L., Cheung, S.W., Yuk, T.I.: Compact multiple-input-multipleoutput antenna using quasi-self-complementary antenna structures for ultrawideband applications. IET Microw. Antennas Propag. **8**(13), 1021–1029 (2014a)

Liu, X.L., Wang, Z., Yin, Y.-Z., Wang, J.H.: Closely spaced dual band-notched UWB antenna for MIMO applications. Progr. Electromagn. Res. C **46**, 109–116 (2014b)

Lodhi, D., Singhal, S.: Pentagon inscribed circular super-wideband fractal MIMO antenna. Int. J. Commun. Syst. (2021). https://doi.org/10.1002/dac.5039

Maity, S., Tewary, T., Mukherjee, S., Roy, A., Sarkar, P.P., Bhunia, S.: Super wideband high gain hybrid microstrip patch antenna. AEU Int. J. Electron. Commun. **153**, 154264 (2022)

Manohar, M., Kshetrimayum, R.S., Gogoi, A.K.: Printed monopole antenna with tapered feed line, feed region and patch for super wideband applications. IET Microw. Antennas Propag. **8**(1), 39–45 (2014)

Mao, C.-X., Chu, Q.-X., Wu, Y.-T., Qian, Y.-H.: Design and investigation of closely-packed diversity UWB slot-antenna with high isolation. Progr. Electromagn. Res. C **41**, 13–25 (2013)

Mohanty, A., Behera, B.R.: Insights on radiation modes and pattern diversity of two element UWB fractal MIMO antenna using theory of characteristics modes analysis. AEU-Int. J. Electron. C. **135**, 153726 (2021)

Mohanty, A., Ranjan Behera, B.: Insights on radiation modes and pattern diversity of two element UWB fractal MIMO antenna using theory of characteristics modes analysis. AEU Int. J. Electron. Commun. **135**, 153726 (2021)

Mushiake, Y.: Self-complementary antennas. IEEE Antennas Propag. Mag. **34**(6), 23–29 (1992)

Mushiake, Y.: A report on Japanese development of antennas: from the Yagi-UDA antenna to self-complementary antennas. IEEE Antennas Propag. Mag. **46**(4), 47–60 (2004)

Nikam, P.B., Kumar, J., Sivanagaraju, V., Baidya, A.: Dual-band reconfigurable EBG loaded circular patch MIMO antenna using defected ground structure (DGS) and PIN diode integrated branch-lines (BLS). Measurement **195**, 111127 (2022)

Okan, T.: A compact octagonal-ring monopole antenna for super wideband applications. Microw. Opt. Technol. Lett. **62**(3), 1237–1244 (2019)

Oni, M. A., Shehab, S. H., Hassan, S., Dey, S.: Design and analysis of a low-profile, elliptical patch super wide band (SWB) Mimo Antenna. In: 2015 International Conference on Advances in Electrical Engineering (ICAEE) (2015)

Patre, S.R., Singh, S.P.: Broadband multiple-input–multiple-output antenna using castor leaf-shaped quasi-self-complementary elements. IET Microw. Antennas Propag. **10**(15), 1673–1681 (2016)

Radhi, A.H., Nilavalan, R., Wang, Y., Al-Raweshidy, H.S., Eltokhy, A.A., Ab Aziz, N.: Mutual coupling reduction with a wideband planar decoupling structure for UWB–Mimo Antennas. Int. J. Microw. Wireless Technol. **10**(10), 1143–1154 (2018)

Raheja, D.K., Kumar, S., Kanaujia, B.K.: Compact quasi-elliptical-self-complementary four-port super-wideband MIMO antenna with dual band elimination characteristics. AEU-Int. J. Electron. Commun. **114**, 153001 (2020)

Sharma, N., Sharma, V., Bhatia, S.S.: A novel hybrid fractal antenna for wireless applications. Progr. Electromagn. Res. M **73**, 25–35 (2018)

Singh, S., Varma, R., Sharma, M., Hussain, S.: Super-wideband monopole reconfigurable antenna with triple notched band characteristics for numerous applications in wireless system. Wireless Pers. Commun. **106**(3), 987–999 (2019)

Singhal, S., Singh, A.K.: CPW-fed hexagonal Sierpinski super wideband fractal antenna. IET Microw. Antennas Propag. **10**(15), 1701–1707 (2016)

Srivastava, K., Kumar, A., Kanaujia, B.K., Dwari, S., Kumar, S.: A CPW-fed UWB MIMO antenna with integrated GSM band and dual band notches. Int. J. RF Microw. Comput. Aided Eng. **29**(1), e21433 (2018)

Toktas, A.: G-shaped band-notched Ultra-wideband MIMO antenna system for mobile terminals. IET Microw. Antennas Propag. **11**(5), 718–725 (2017)

Ur Rahman, S., Cao, Q., Wang, Y., Ullah, H.: Design of wideband antenna with band notch characteristics based on single notching element. Int. J. RF Microw. Comput. Aided Eng. **29**(2), e21541 (2018)